Food and Chemical Toxicology 112 (2018) 383–392

Contents lists available at ScienceDirect

Food and Chemical Toxicology

journal homepage: www.elsevier.com/locate/foodchemtox

Apoptosis induction by *Pleurotus sajor-caju* (Fr.) Singer extracts on colorectal cancer cell lines

Tiane C. Finimundy[a,c], Rui M.V. Abreu[c], Natalia Bonetto[a], Fernando J. Scariot[b], Aldo J.P. Dillon[d], Sergio Echeverrigaray[b,1], Lillian Barros[c], Isabel C.F.R. Ferreira[c,*], João A.P. Henriques[a], Mariana Roesch-Ely[a,**]

[a] Laboratory of Genomics, Proteomics and DNA Repair, Institute of Biotechnology, University of Caxias do Sul, Caxias do Sul, Brazil
[b] Laboratory of Applied Microbiology, Institute of Biotechnology, University of Caxias do Sul, Caxias do Sul, Brazil
[c] Centro de Investigação de Montanha (CIMO), Instituto Politécnico de Bragança, Campus de Santa Apolónia, 5300-253 Bragança, Portugal
[d] Laboratory of Enzyme and Biomass, Institute of Biotechnology, University of Caxias do Sul, Caxias do Sul, Brazil

ARTICLE INFO

Keywords:
Pleurotus sajor-caju
Sterols
Cytotoxicity
Apoptosis

ABSTRACT

Pleurotus sajor-caju (PSC) is an edible mushroom used in food supplements, presenting antitumor properties through induction of cell death pathways. The PSC potential against colorectal cancer was analyzed by exposing HCT116^{wt} cells to different PSC extracts. The PSC n-hexane extract (PSC-hex) showed the highest cytotoxicity effect (IC_{50} value 0.05 mg/mL). The observed cytotoxicity was then associated to apoptosis-promoting and cell cycle-arrest pathways. PSC-hex was able to induce apoptosis related to breakdown of mitochondrial membrane potential and ROS generation. The absence of cytotoxicity in HTC116^{-p53} and HTC116^{-Bax} cells, alongside with an increase in p53, Bax and Caspase-3 expression, and decrease in Bcl-2 expression, supports that the pro-apoptotic effect is probably induced through a p53 associated pathway. PSC-hex induced cell cycle arrest at G2/M in HCT116^{wt} without cytotoxicity in HTC116^{-p21} cells. These findings suggest that a p21/p53 cell cycle regulation pathway is probably disrupted by compounds present on PSC-hex. Identification of the major components was then performed with ergosta-5,7,22-trien-3β-ol representing 30.6% of total weight. In silico docking studies of ergosta-5,7,22-trien-3β against Bcl-2 were performed and results show a credible interaction with the Bcl-2 hydrophobic cleft. The results show that PSC-hex can be used as supplementary food for adjuvant therapy in colorectal carcinoma.

1. Introduction

Colorectal cancer (CRC) is the third most common type of cancer and fourth leading cause of cancer death in the world as about 690,000 people annually die for this disease (Arnold et al., 2017). Clinically, chemotherapy and radiation are commonly used before or after surgery, even so 40% of all patients develop metastasis and presented recidives (Bahrami et al., 2018). CRC is classified by its clinicopathological characteristics, but clinical outcomes and drugs response, molecular characteristics and prognosis are uncertain and heterogeneous (Rodriguez-Salas et al., 2017). The molecular changes associated to tumor progression are attributable to genomic instability that shows common alteration of critical pathways. These include TP53, PI3CA, TGF-β, and Epithelial-to-mesenchymal transition (EMT) genes. These molecular events allows modifications such as loss of control of cell growth, increases cell-survival and cell-proliferation, promotes invasion, inhibits apoptosis, promotes epithelial to mesenquimal-transition and angiogenesis (Rodriguez-Salas et al., 2017).

The identification of consensus molecular subtypes (CMS) have clinical relevance independent of cancer stage and is heavily influenced by the tumor microenvironment, are divided into CMS1 (MSI immune), CMS2 (canonical), CMS3 (metabolic) and CMS4 (mesenchymal). These CMS subtypes are represented *in vitro* model systems, providing resource for preclinical studies in CRC (Berg et al., 2017). CMS4 tumors tended to be diagnosed at more advanced stages (III and IV), and one of the cell lines representing *in vitro* this subtype is HCT116.

Therefore there is a constant demand to investigate new and effective anti-CRC drugs to improve survival while maintaining health-related quality of life (Quidde et al., 2016; Rejhová et al., 2017). Diet appears to be one of the ways by which carcinogenic agent instigate the

* Corresponding author.
** Corresponding author.
E-mail addresses: iferreira@ipb.pt (I.C.F.R. Ferreira), mrely@ucs.br (M. Roesch-Ely).
[1] Cytogenes Diagnostics Biology Ltda.

https://doi.org/10.1016/j.fct.2018.01.015
Received 4 December 2017; Received in revised form 9 January 2018; Accepted 10 January 2018
Available online 11 January 2018
0278-6915/

DNA repair modulating the intensity of early carcinogenic events (Rejhová et al., 2017). Several natural chemopreventive food compounds are being evaluated as edible and medicinal supplements, including the ones found in mushrooms, with antitumor substances already been identified in many species (Alonso et al., 2017; Gogavekar et al., 2014; Jin et al., 2016; Santesso and Wieland, 2016). Antiproliferative activity of *Pleurotus sajor-caju* (Fr) Singer extracts against human tumor cell lines (Hep-2, HeLa, Sarcoma 180, among others) has been reported (Assis et al., 2013). There is a major interest in the use of mushrooms and/or extracts as dietary supplements, given the beneficial properties as enhancers of immune function and promoters of health (Lo et al., 2012; Roncero-Ramos and Delgado-Andrade, 2017; Tanaka et al., 2016).

Different molecules found in fruiting bodies have been reported to present antitumor potential (Greeshma et al., 2016; Ren et al., 2012). Some examples are polysaccharides, glycoproteins, proteoglycans, proteins, quinones, cerebrosides, isoflavones, catechols, triacylglycerols, phenolic acids, terpenes, and steroids (Ferreira et al., 2010; Villares et al., 2012). Evidences support the theory of antitumoral properties of sterols, including inhibition of tumor growth and stimulation of apoptosis (Kikuchi et al., 2017). According to Barreira and Ferreira (2015), the mechanism underlying the inhibition of cell growth could be similar to the mechanism associated with protein kinase C activity. Understanding the mechanism of apoptosis has important implications in the prevention and treatment of many diseases, in particular cancer. The Bcl-2 family of proteins are apoptotic regulators that control cell survival (Opferman and Kothari, 2018).

So, it is important to explore how *Pleurotus sajor caju* (PSC) constituents may regulate the cell dynamics and reduce cell proliferation. Identification of isolated compounds or extracts that induce the apoptotic cascade to reduce proliferation rates of cancer cells would be an effective strategy to control cancer progression (Venkatesh Gobi et al., 2018). The aim of this study was to investigate the effect of PSC extracts, specifically the PSC n-hexane extract (PSC-hex) in the proliferation of colorectal cancer cells (HCT116^{wt}, $^{-Bax}$, $^{-p21}$ and $^{-p53}$), and to correlate the observed anti-proliferation activity to activation of pro-apoptotic and/or cell arrest regulation pathways. To verify cell selectivity, MRC-5 cell line was used, a lung fibroblast cell line origin that is associated with the initiation of epithelial-mesenchymal transition and metastasis. The identification of the main PSC -hex components was also obtained, and *in silico* docking studies were performed to provide clues on the potential mechanism of action of the PSC n-hexane extract by the inhibition of the Bcl-2, an anti-apoptotic protein.

2. Material and methods

2.1. Experimental materials

Trypsin and RNase A were from Gibco Invitrogen Co. (Paisley, UK). Dulbecco's Modified Eagle Medium (DMEM) and fetal bovine serum (FBS) were acquired from Hyclone Lab Inc. (USA). Acetic acid, dimethylsulfoxide (DMSO), propidium iodide (PI) and phenolic standards were from Sigma Chemical Co. (St. Louis, USA). DiOC6(3) (3,3′-Dihexyloxacarbocyanine Iodide (TermoFisher, Eugene,OR). Dichlorodihydrofluorescein (DCFH) and DAPI 4′,6-diamidino-2-phenylindole were purchased from Sigma-Aldrich (St. Louis, USA). Tricloroacetic acid (TCA) and Tris-Base were from Merck (Darmstadt, Germany). Folin-Ciocalteu's phenol reagent (Merck) was used for the determination of total phenols. All standards were purchased from Sigma-Aldrich, FITC Annexin V Apoptosis Detection Kit (Sigma-Aldrich, MO, USA), anti-Bax (Abcam, 1:500), anti-BCl-2 (Abcam, 1:500), anti-caspase-3 (Abcam, 1:500), anti-β-actin (Abcam, 1:1000), Human Apoptosis Antibody Array Kit (Abcam).

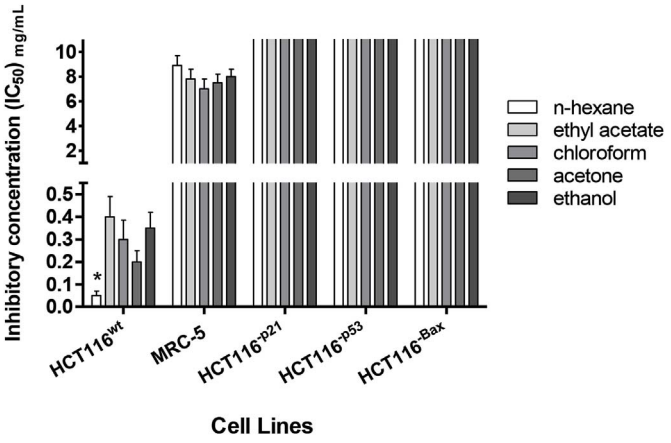

Fig. 1. Results the cytotoxic effect from MTT assay after 24 h incubation for the different extracts in HCT116^{wt}, HCT116^{-Bax}, HCT116^{-p53} and HCT116^{-p21} cell lines and lung human cell line (MRC-5). Data are the mean ± S.D. of three independent experiments. * $p < .05$ versus control.

2.2. Sample preparation

Samples of *Pleurotus sajor-caju* fruiting bodies (edible mushrooms) were collected in farm located 29°09′48.9″S 51°36′56.5″W, at Rio Grande do Sul state, in the southern region of Brazil, in autumn 2015. The extracts were obtained using an ultrasonic device (QSonica sonicators, model CL-334, Newtown, CT, USA), comprising an ultrasound power of 500 W, at a frequency of 20 kHz, equipped with a digital timer, following a protocol previously described by Heleno et al. (2016). The lyophilized powdered samples (10 g) were extracted with 100 mL of each selected solvent (n-hexane, chloroform, ethyl acetate, ethanol and ethanol/water (1:1, v/v)) into the ultrasonic device at the temperature of 20 °C, for 30 min. After extraction, the mixture was filtered and the solvent lyophilized. For the cytotoxicity assay, five dried extracts obtained were dissolved in ethanol/water (25:75, v/v).

2.3. Cell culture

HCT116^{wt} and MRC-5 cells were acquired from ATCC (American Type Culture Collection, United States), and HCT116^{-Bax}, HCT116^{-p21}, HCT116^{-p53} were supplied by Dr. Annette K. Larsen (Laboratory of Cancer Biology and Therapeutics, Paris, France). All the reagents were of ultrapure grade. Water was treated in a Milli-Q water purification system (TGI Pure Water Systems, USA). HCT116^{wt} (human colorectal carcinoma), HCT116^{-Bax}, HCT116^{-p21}, HCT116^{-p53} and MRC-5 (Fibroblast lung) were routinely maintained as adherent cell cultures in DMEM medium with 10% heat-inactivated FBS, in a humidified incubator at 37 °C with 5% CO_2. Cell cultures were periodically tested for Mycoplasma contamination. HCT116 cell lines were authenticated at DNA Diagnostics Center (DDC) from Public Health England (PHE) using short tandem repeat (STR) methodology and reference sample comparison to ATCC STR profile database. All assays were performed with cells in exponential growth, with viabilities over 90% and repeated at least in three independent experiments.

2.4. Cell viability (MTT assay)

All cells were evaluated according to the procedure adopted in the NCI's (National Cancer Institute) *in vitro* anticancer drug screening, which uses MTT assay to assess cell survival (Denizot and Lang, 1986). Briefly, the cell line was plated at an appropriate density (5×10^4 cells/well) in 96-well plates and allowed to attach for 24 h. Cells were then treated for 24 h with various concentrations of the extracts. Following this period, the adherent cells were incubated with MTT for 2 h. The crystal formazan was solubilized with DMSO and the absorbance was

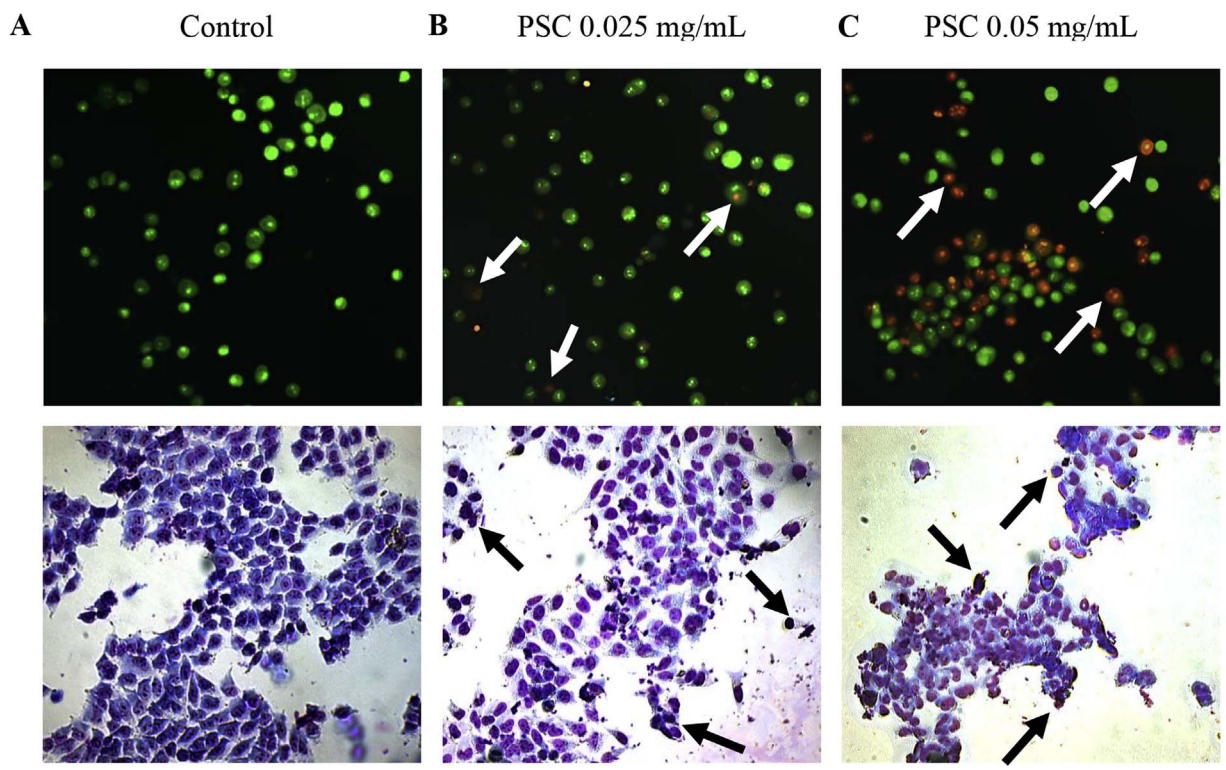

Fig. 2. Results dual stain OA/EB and Giemsa in HCT116^{wt} cell line. (A). Negative control (ethanol) group: circular green nucleus uniformly distributed in the center of the cell. (B) PSC 0.025 mg/mL (early apoptotic cells): nucleus showed yellow-green fluorescence staining and concentrated into a crescent or granular shape. (C) PSC 0.05 mg/mL (late apoptotic cells): the nucleus of cell showed orange or red fluorescence staining and gathered in concentration and located in bias and necrotic cells volume was increased, showing uneven red fluorescence and an unapparent outline. and the color observed after fluorescence staining in red indicate late apoptosis and yellow early events of apoptosis. (For interpretation of the references to color in this figure legend, the reader is referred to the Web version of this article.)

measured at 540 nm in a microplate reader SpectraMAX M2/M2e (Molecular Devices, USA). The anti-proliferative activity of the compounds was inferred from the MTT assay by comparing the absorbance of the wells containing extract-treated cells with the absorbance of the wells containing untreated cells (Tolosa et al., 2015). Three to six independent experiments were performed in duplicate, the results were expressed as mean values ± standard deviation (SD) and IC_{50} (dose causing 50% cell death).

2.5. Acridine orange/ethidium bromide staining

The changes in chromatin organization, apoptotic cells or fragmented nuclei upon treatment with PSC-hex was determined microscopically by acridine/orange-ethidium bromide (AO-EB) dual staining. HCT116 cells (7×10^4 cell/well) were grown in 24-well plates. After 24 h of extract treatment, the cells were detached and the suspension from each well was separated in vials. The vials were centrifuged at 1200 rpm for 5 min. The pellet obtained was washed once with PBS, stained with AO/EB solution with 25 µL PBS and 2 µL AO/EB dye, incubated for 5 min, and observed under fluorescence microscope (BX43 - Olympus). Morphological changes were determined according to Pajaniradje et al. (2014).

2.6. ROS accumulation and mitochondrial membrane potential ($\Delta\psi m$) measurement

Reactive Oxygen Species (ROS) generation was analyzed by flow cytometry using DCFH-DA. Cells were treated with PSC-hex for 24 h, suspended in PBS and incubated with 10 µM DCFH-DA at 37 °C for 30 min. Fluorescence generation due to the hydrolysis of DCFH-DA to dichlorodihydrofluorescein (DCFH) by non-specific cellular sterases, and the subsequent oxidation of DCFH by peroxides was measured by means of flow cytometry (BD FACScalibur, San Jose, California). The uptake of the cationic fluorescent dye 3,3′-dihexyloxacarbocyanine iodide (DiOC6(3)) (2 µL of 2 µmol/L stock solution in dimethyl sulfoxide [DMSO]) was used for the evaluation of mitochondrial membrane potential (Aranda et al., 2013). Cell treatment was performed as in ROS experiments. Untreated controls and treated cells were harvested and washed twice with PBS. The cell pellets were then re-suspended in 2 mL of fresh incubation medium containing DiOC6 and incubated at 37 °C in a thermostatic bath for 30 min. HTC116 cells were separated by centrifugation, washed twice with PBS, and analyzed by flow cytometry using FL1 channel (488/533 nm) (BD FACScalibur, San Jose, Califórnia) (Wlodkowic et al., 2009).

2.7. Apoptosis and cell cycle analysis by flow cytometry

Induced apoptosis was assayed by the Human Annexin V-FITC/PI apoptosis Kit (Sigma-Aldrich, MO, USA), according to the manufacturer's instructions. The fraction of the cell population in different quadrants was measured using quadrant statistics with the FlowJo 10.0 software (LLC, Ashland, Ore). For the analysis of cell cycle phase distribution, HCT116^{wt} cells were plated at 1.5×10^5 cells/mL in 6-well plates and left incubating for 24 h. Cells were then incubated with complete medium only, medium with the control solvent ethanol/water (25:75 v/v) or with PSC-hex at IC_{50} (0.05 mg/mL) and half IC_{50} (0.025 mg/mL), previously determined by the MTT assay (Monks et al., 1991). Cells were harvested following 24 h incubation with the extract and further processed for either cell cycle analysis or apoptosis detection. For cell cycle analysis, cells were fixed in 70% ethanol for 10 min at room temperature. After centrifugation cells were incubated with PI (5 µg/mL) and RNase A in PBS (100 µg/mL) for 30 min on ice (Pozarowski and Darzynkiewicz, 2004). Cellular DNA content (for cell cycle distribution analysis and presence of sub-G1 peak, suggestive of

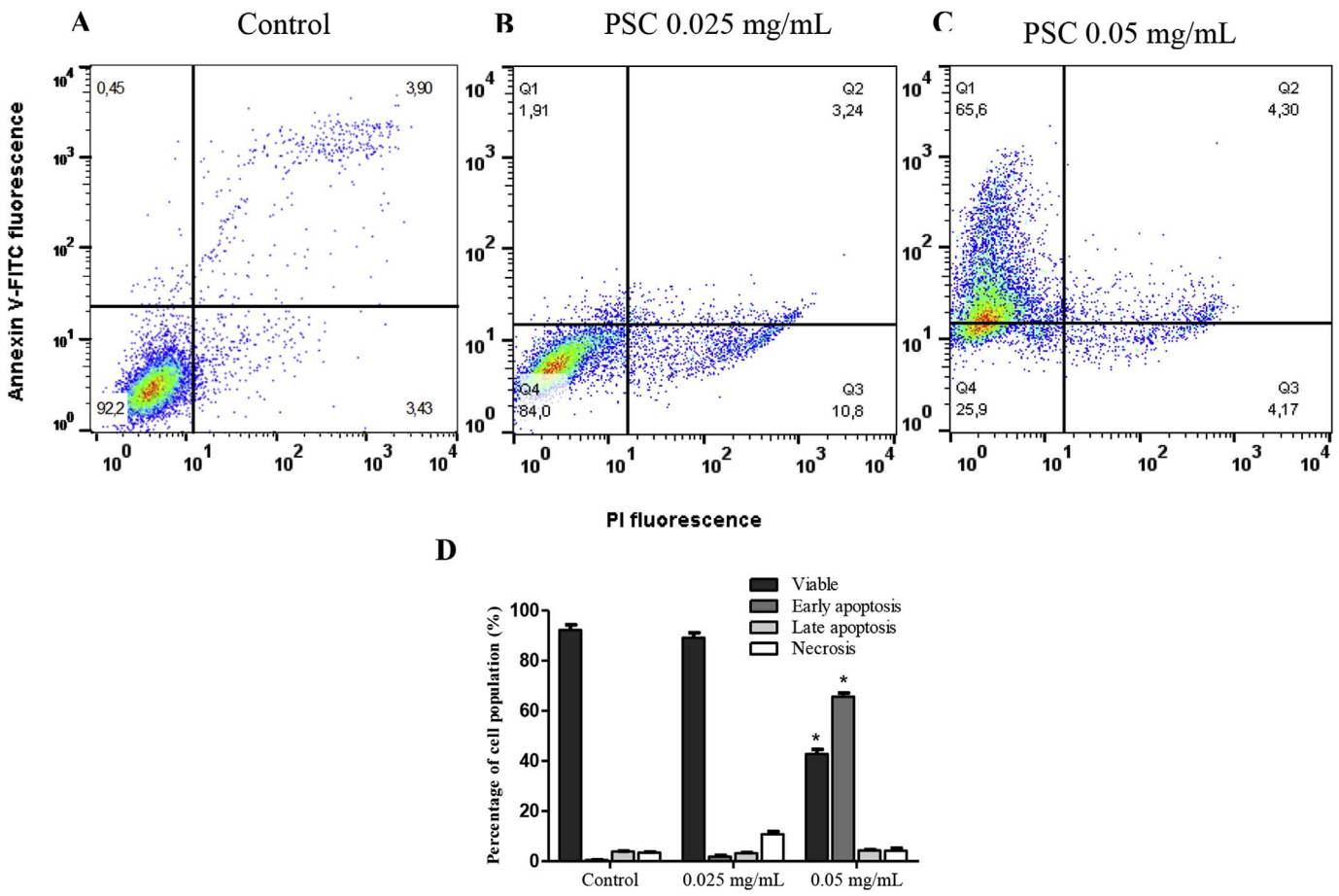

Fig. 3. Apoptosis analysis in HCT116^{wt} cells using annexin V-FITC/PI though cytometry analysis for control and treated samples. The early apoptotic events (Annexin + /PI-) are shown in lower right quadrant (Q1) of each panel. Quadrant (Q3) represents Annexin + /PI + late stage of apoptosis/necrosis. A) Control; (B, C) treatment with 0.025 mg/mL and 0.05 mg/mL of PSC respectively. D) Quantitative results from flow cytometry. Results are the mean ± SD of three to six independent experiments performed in duplicate. *Values statistically significantly ($P < .05$) different when compared to blank.

apoptosis induction) and measurement of phosphatidylserine externalization were analyzed using FL1 channel (488/533 nm) and FL3 channel (488/670 nm) an BD FACScalibur, San Jose, Califórnia, plotting at least 10,000 events per sample (Pietkiewicz et al., 2015). Three to six independent experiments were performed in duplicate and the results were expressed as mean values ± standard deviation (SD). ρ values < 0.05 were considered as statistically significant.

2.8. Apoptosis antibody array membranes analysis

Relative levels of 43 human apoptosis-related proteins were detected and analyzed using a human array kit, according to the manufacturer's instructions (Abcam, #ab134001). Briefly, the membrane containing immobilized apoptosis-related antibodies was blocked with bovine serum albumin for 2 h on a rocking platform at room temperature. The membrane was then incubated with lysates of untreated or treated HCT116^{wt} cells (IC_{50}), along with Detection Antibody Cocktail overnight at 2 °C to 8 °C. The membrane was incubated with streptavidin horseradish peroxidase conjugate followed by chemiluminescent detection reagent. The membrane was scanned using ImageQuant LAS 500 (GE Healthcare life sciences). According Schneider et al. (2012) the pixel density in each spot volume was determined, corrected for background and expressed as fold change (treated vs. untreated cells) using ImageJ version 1.46 software (NIH, Bethesda, MD; http://imagej.nih.gov/ij). Protein Array Analyzer plugin (available at image.bio.methods.free.fr/ImageJ/?Protein-Array-Analyzer-for-ImageJ.html, last accessed Oct 8, 2015) (Carpentier, 2014).

2.9. Western blotting analysis

To evaluate the expression levels of intracellular proteins related to apoptosis, HCT116^{wt} cells were treated with PSC-hex (IC_{50}) for 24 h. For the isolation of total protein fractions, the cells were collected, washed twice with ice-cold PBS, and lysed using cell lysis buffer (NP40, 20 mM Tris pH 7.5, 150 mM NaCl, 1% Triton X-100, 2.5 mM sodium pyrophosphate, 1 mM EDTA, protease inhibitor). The lysates were collected by scraping from the plates and then centrifuged at 10,000 rpm at 4 °C for 5 min. Total protein samples were loaded on a 12% of SDS polyacrylamide gel electrophoresis and transferred onto polyvinylidene fluoride (PVDF) membrane (Millipore, Billerica, MA, USA) for 1 h. Membranes were blocked at room temperature for 1 h with blocking solution (5% power milk in TBST). Next, the membranes were incubated for 1 h at room temperature with antihuman Bcl-2 rabbit pAb (1:1000 dilution; Abcam), antihuman Bax rabbit pAb (1:1000 dilution; Abcam), antihuman Caspase-3 rabbit pAb (1:500 dilution; Abcam) or antihuman β-actin mouse (1:1500). After washing, the membranes were incubated for 1 h at room temperature with horseradish peroxidase (HRP)-linked antimouse Ig (1:1000 dilution; Amersham) for β-actin or HRP-linked antirabbit Ig (1:50,000 dilution; Amersham) for Bax, Bcl-2 and Caspase-3. Immunoblots were performed using ECL prime Western blotting detection kit (Amersham). Chemiluminescence visualization and detection was performed using ImageQuant LAS 500 (GE Healthcare life sciences).

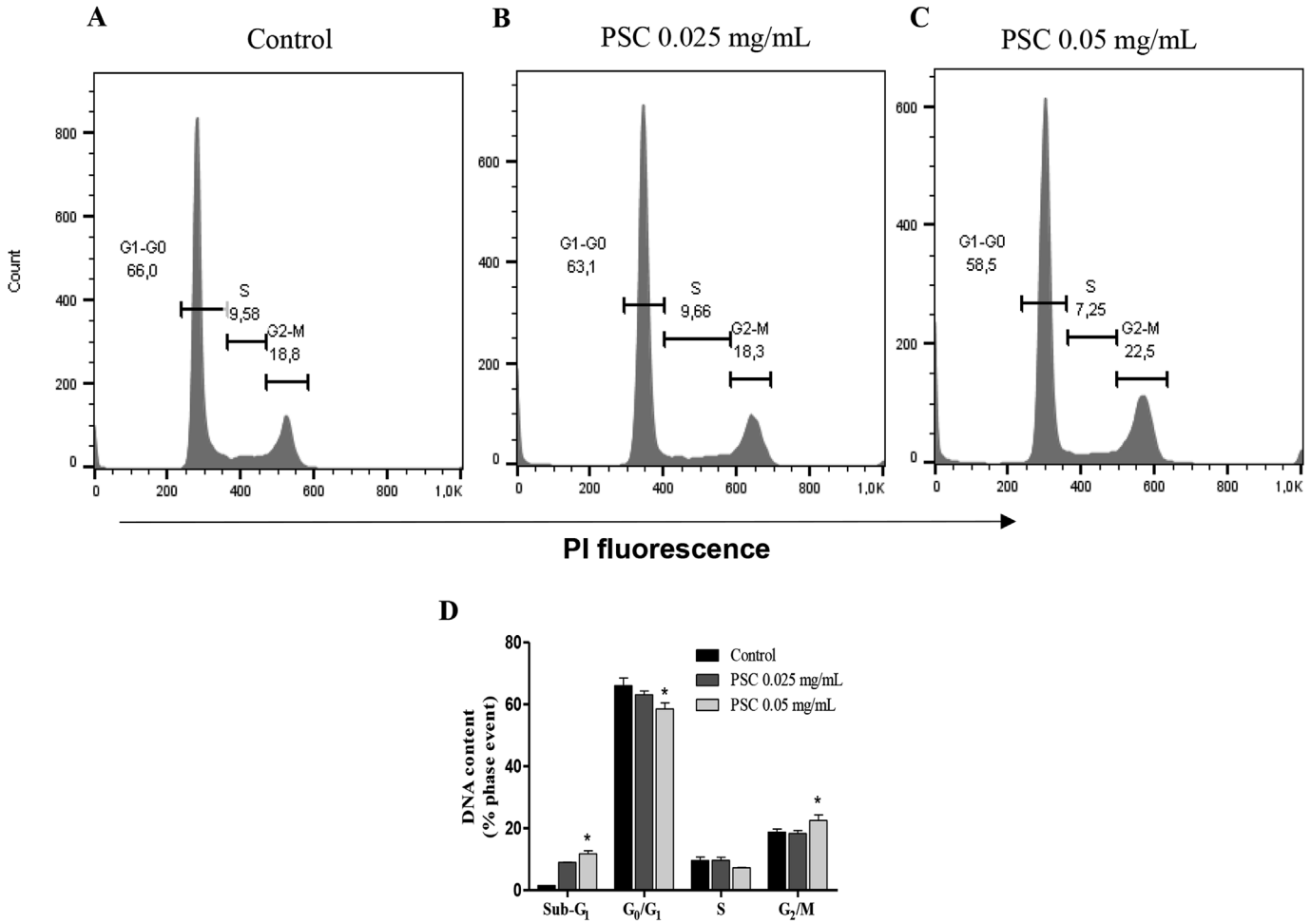

Fig. 4. Cell cycle distribution percentage of HCT116^{wt} cells after treatment with different concentrations of PSC (B,C) compared to control (A). The results of the cell cycle distribution analysis by flow cytometry were analyzed by ModFit. D) The percentages of cell populations of different cell cycle phases are shown. Results are the mean ± SD of three to six independent experiments performed in duplicate. *Values statistically significantly ($P < .05$) different when compared to blank.

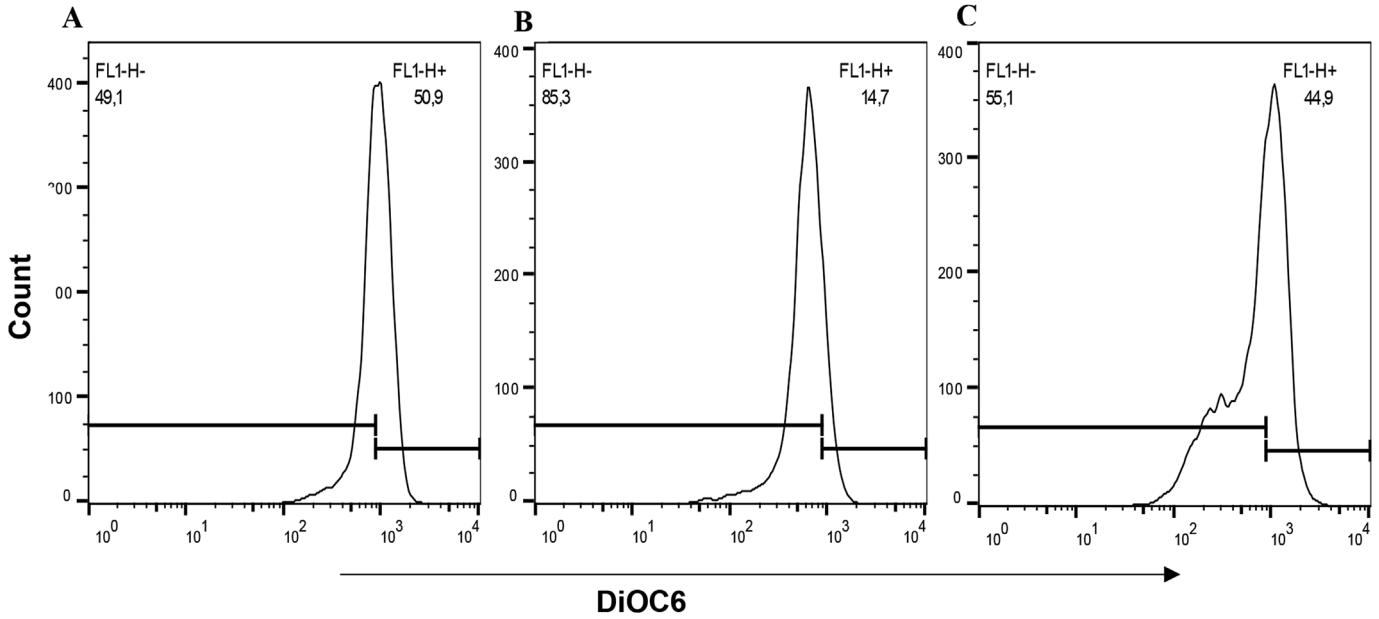

Fig. 5. Mitochondrial membrane potential of HCT116^{wt} cells after treatment with extracts of mushrooms using DiOC6(3) staining through cytometry. Cells with decreased fluorescence (increase to the left of the graph), present mitochondria depolarization A) Control; (B, C) treatment with 0.025 mg/mL and 0.05 mg/mL of PSC, respectively. Results are the mean ± SD of three to six independent experiments performed in duplicate.

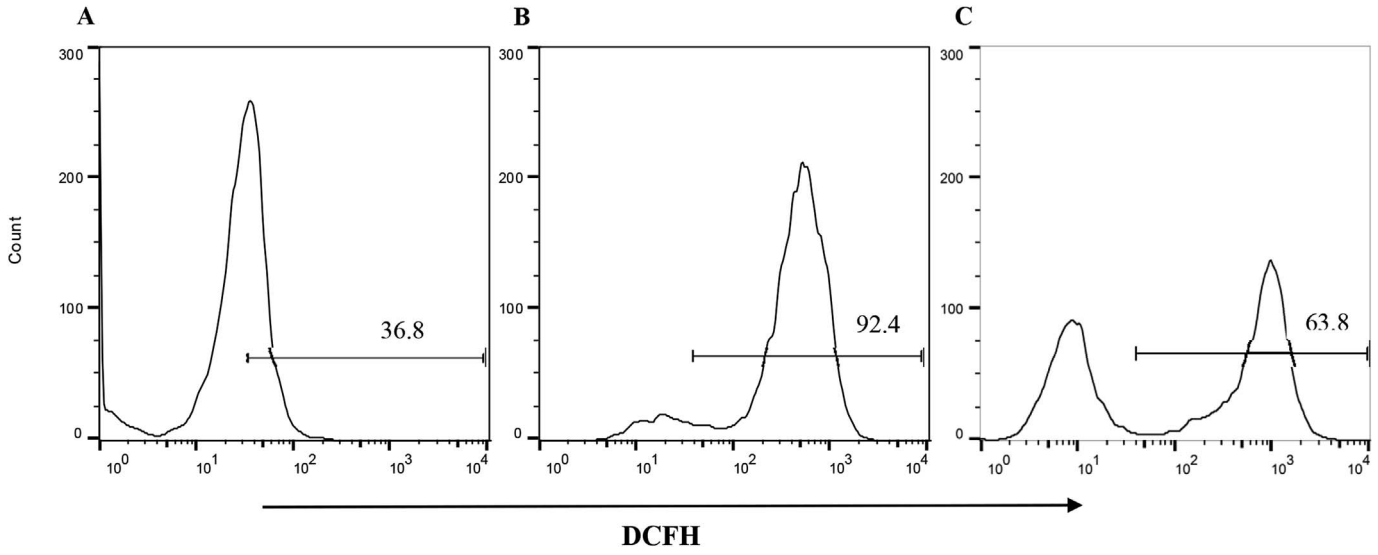

Fig. 6. Cytometry evaluation indicating ROS formation in HCT116^{wt} cells before and after extract exposition. Cells with increased fluorescence (increase to the right of the graph), present accumulation of ROS A) Control; (B, C) treatment with 0.025 mg/mL and 0.05 mg/mL of PSC, respectively. Results are the mean ± SD of three to six independent experiments performed in duplicate.

2.10. Gas chromatography-mass spectrometry (GC-MS)

PSC-hex was chemically characterized by GC-MS after sample derivatization. This process consisted on the derivatization of hydroxyl and carboxyl groups of the extracted compounds with 300 µL of *N,O*-bis (trimethylsilyl)trifluoroacetamide (BSTFA; PanReac AppliChem, Barcelona, Spain) by heating the resulting mixture at 70 °C for 1 h prior to analysis. The derivatized sample was analyzed by GC-MS following a protocol previously described by Falcão et al. (2016), consisting on a Perkin Elmer system with a Clarus® 580 GC module and a Clarus® SQ 8 S MS module, equipped with DB-5MS fused-silica column (30 m × 0.25 mm i.d., film thickness 0.25 µm; J & W Scientific, Inc.). Oven temperature was programmed, 45–175 °C, at 3 °C/min, subsequently at 15 °C/min up to 300 °C, and then held isothermal for 10 min; injector and detector temperatures were 280 °C. The transfer line temperature was 280 °C; ion source temperature, 220 °C; carrier gas, helium, adjusted to a linear velocity of 30 cm/s; split ratio, 1:40; ionization energy, 70 eV; scan range, 40–300 u; scan time, 1 s. The software Turbomass (software version 6.1.0, Perkin Elmer, Shelton, CT, USA) for Windows was used for data acquisition. The identity of the components was assigned by comparison of their retention indices, relative to C7-C40 n-alkane indices and GC-MS spectra from a commercial MS database (NIST).

2.11. Molecular docking

A Bcl-2 crystal structure was selected and obtained from the Protein Data Bank (PDB entry: 4LXD). The Bcl-2 protein structure was prepared for docking by removing all crystallized water molecules and the Venetoclax inhibitor. AutoDockTools1.5.2 (ADT) (Morris et al., 2008) was then used to assign polar hydrogens, add Gasteiger charges and save the protein structure in PDBQT file format. A docking grid was selected using ADT in order to encompass completely the ligand binding site. The X,Y,Z grid center coordinates selected were 23.3, 32.7 and 13.1 respectively, and the X,Y,Z grid dimensions used were of 20 by 20 by 20 Å. The 2D structure of the studied sterol (Ergosta-5,7,22-trien-3β-ol), was drawn using ACD/ChemSketch Freeware 12.0 software. VegaZZ software was then used to perform 2D to 3D conversion and to save the structures in PDB file format (Pedretti et al., 2004). Finally, ADT was used to convert PDB to PDBQT file format. All docking simulations were performed using AutoDock Vina software (Trott and Olson, 2010), using an exhaustiveness parameter of 32. Docking conformation analysis and image preparation was performed using PyMOL software (Delano, 2002).

2.12. Statistical analysis

All of the data were expressed as mean ± SD. Differences between groups were determined by using the Student's *t*-test, and different groups were compared using one-way ANOVA followed by Tukey multiple comparison to evaluate the differences between two groups under multiple conditions. Statistical analysis was performed using SPSS21.0 software. $P < .05$ was considered statistically significant.

3. Results and discussion

3.1. PSC extract exhibited anti-proliferative activity against the HCT116^{wt} cells

In order to evaluate the anti-proliferative activity of PSC, five cell lines (HCT116^{wt}, HCT116^{-Bax}, HCT116^{-p21}, HCT116^{-p53} and MRC-5) were exposed to different concentration of PSC extracts for 24 h using a variation of solvent polarity (hexane, chloroform, ethyl acetate, ethanol and ethanol/water (1:1)). According Joana Gil-Chávez et al. (2013), these organic solvents can be used for the extraction of both polar and nonpolar compounds such as fatty acids, alkaloids, organochlorine, phenols, aromatic hydrocarbons and oils, among others. As shown in Fig. 1 a batch of different conditions crude extract were investigated. The results revealed PSC n-hexane extraction as the most promising condition, with an IC_{50} value of 0.05 mg/mL in HCT116^{wt} followed by PSC acetone extract with an IC_{50} value of 0.2 mg/mL. This result is probably due to the amount of lipophilic compounds extracted in this extract, corroborating with Sang et al. (2006) that they also presented better activity against human cancer cells including colon carcinoma (Caco-2), breast carcinoma (MCF-7) and acute myeloid leukemia (HL-60) cells. The other extracts might require very high concentrations to obtain the same effect as the n-hexane extract, which would make it unusable.

Interestingly, while the PSC-hex was able to induce cytotoxic effects on human colorectal carcinoma cells (HCT116^{wt}), it showed practically no anti-proliferative activity in non-tumor MRC-5 cells (Fig. 1). The anticancer activity of the n-hexane extract was attributed to high sterol content. Their selectivity may be related to inhibition of the mitochondrial complex I, which according to Kalyanaraman et al. (2018),

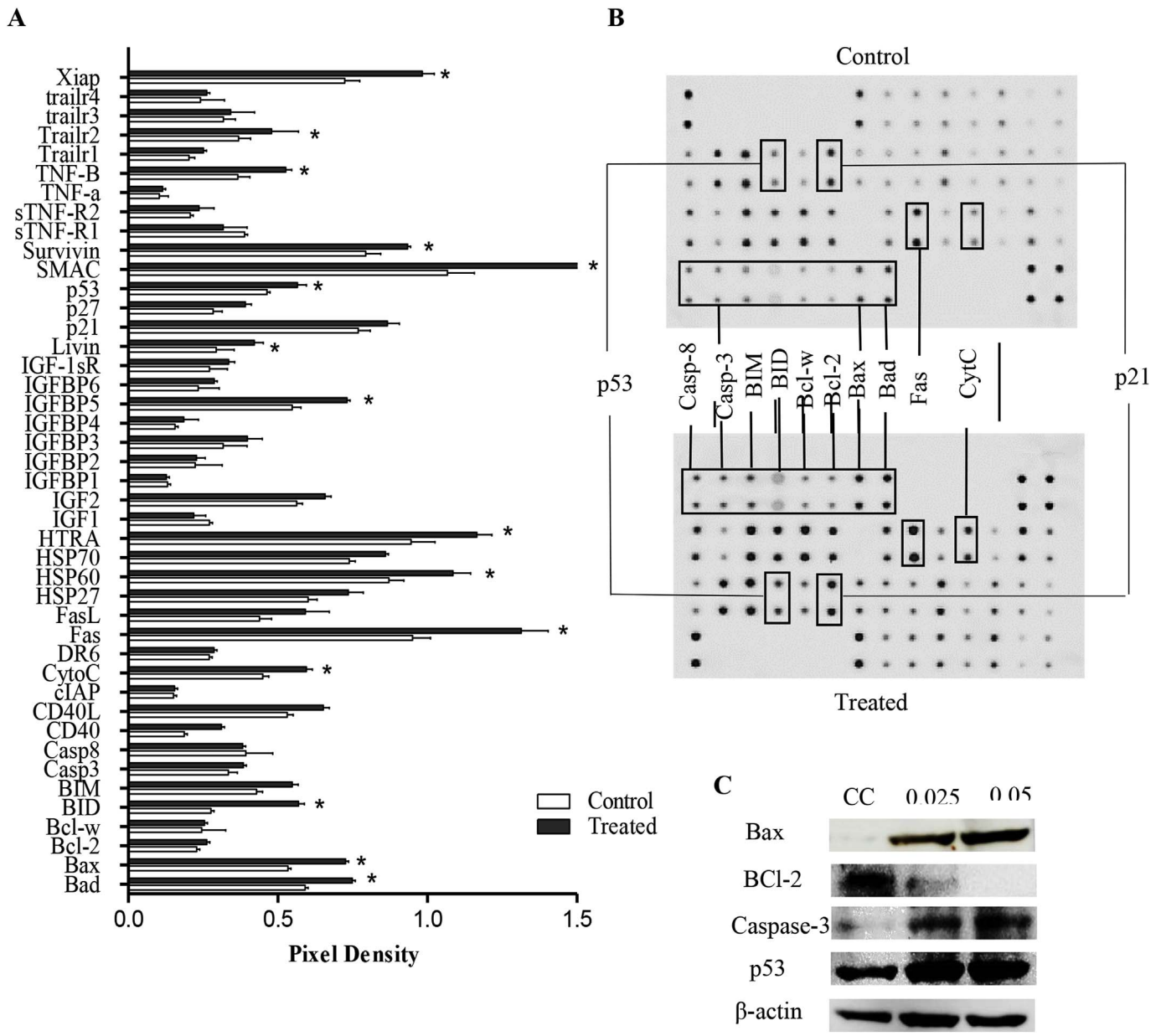

Fig. 7. Modulation of apoptosis-related proteins before and after PSC extract exposition in HCT116^{wt} cells treatment with 0.025 and 0.05 mg/mL A) Pixel densities of apoptosis-related proteins identified from array analysis of HCT116^{wt} cell in response to treatment of 24 h at a concentration of 0.05 mg/mL, showing changes in levels of apoptosis protein compared to untreated group *ρ < 0.05. B) Template demonstrating the location of spots of treated (below) and untreated (above) cell sample group representing the 43 apoptosis-related proteins and location of the spots of the expression apoptosis-related proteins, C) Western blotting showing the expression levels of the proteins. For normalization of protein levels was used β-actin loading control. Results are the mean ± SD of three to six independent experiments performed in duplicate. *Values statistically significantly (P < .05) different when compared to blank.

lipophilic compounds may be a class of therapeutic drugs that inhibit mitochondrial bioenergetics, mitochondrial respiration in tumor cells at relatively non-toxic concentrations. These experiments suggest that the PSC-hex promotes its cytotoxicity by inhibiting tumor-associated signaling pathways. This assumption was tested by performing the same experiments using HCT116 cell lines with deleted tumoral-associated proteins: Bax (HCT116^{-Bax}), p21 (HCT116^{-p21}) and p53 (HCT116^{-p53}). The results were drastic, with no observed anti-proliferation activity on any HCT-116 protein deficient cell lines, after exposure to PSC extracts (Fig. 1). These results suggest that the PSC-hex components disrupt multiple tumoral signaling pathways, including growth arrest (associated to proteins p21 and p53) and/or apoptosis pathways (associated to proteins Bax, Bcl-2 and p53). These results are in line with recent findings, showed that many natural compounds found in mushrooms have pro-apoptotic activities (Yang et al., 2016). Moreover, literature supports that mushroom constituents such as sterols may contribute to the antitumoral effects observed in this study (Heleno et al., 2015). Considering these results, the follow up studies were all performed using 0.05 mg/mL (IC_{50} value) and 0.025 mg/mL (half the IC_{50} value) concentrations of the PSC-hex applied to HCT116^{wt} adenocarcinoma model cell line.

3.2. PSC-hex effect on apoptosis and cell cycle in HCT116^{wt}

Apoptotic programmed cell death is characterized by various morphological and biochemistry changes (Hird et al., 2015). To evaluate the effect of PSC-hex in inducing apoptosis and changes in cell morphology, the Giemsa and OA/EB staining protocol was used, after exposition of HCT116^{wt} cells to 0.025 and 0.05 mg/mL of extract concentration (Liu et al., 2015). Few early-stage apoptotic events were

Table 1
Identification of the compounds present in *P. sajor-caju* non-polar extract (relative abundance %, mean ± standard deviation).

Peak	Identification	RT (min)	LRI	Peak Area (%)
1	Tetradecanoic acid (myristic acid; C14:0)	43.56	1839.14	0.19 ± 0.01
2	D-Mannitol	45.25	1630.50	2.9 ± 0.1
3	Butane	45.38	1738.83	2.67 ± 0.04
4	N-Pentadecanoic acid (C15:0)	45.64	1865.77	3.48 ± 0.09
5	Hexadecanoic acid (palmitic acid, C16:0)	46.98	2021.41	23.2 ± 0.1
6	(z)-9-octadecenoic acid (oleic acid, C18:0)	47.34	1980.35	0.32 ± 0.01
7	Octanoic acid (caprylic acid, C8:0)	47.90	2122.40	0.246 ± 0.003
8	9,12-Octadecadienoic acid (linoleic acid)	48.48	2189.84	24.81 ± 0.03
9	(z)-9,17-Octadecadienal	50.16	2085.69	1.95 ± 0.05
10	Cyclopenta[a.d]cyclo-octen-5-one	50.90	2554.49	0.21 ± 0.01
11	D-(+)-Trehalose	51.52	1940.12	1.34 ± 0.05
12	3,7,11,15-tetramethylhexadeca-2,6,10,14-tetraen-1-ol	51.98	2506.66	0.391 ± 0.005
13	2-α-Mannobiose	52.20	1955.18	1.25 ± 0.03
14	α-D-Glucopyranosiduronic acid	53.05	1974.00	0.96 ± 0.02
15	9(11)-Dehydroergosteryl benzoate	53.19	3275.92	0.44 ± 0.01
16	3α,5α-Cyclo-ergosta-7,9(11),22-triene-6β-ol isomer 1	54.57	3194.11	0.220 ± 0.008
17	Ergosta-5,7,9(11),22-tetraen-3-yl 4-methylbenzenesulfonate	54.68	3316.01	0.78 ± 0.03
18	Ergosta-5,7,22-trien-3β-ol	55.43	3338.31	30.6 ± 0.4
19	3β,22E-ergosta-7,22-dien-3	55.51	3225.26	0.99 ± 0.01
20	Cholesta-5,7-dien-3-ol acetate (3β)	55.90	3340.14	1.28 ± 0.07
21	Cholestan-26-oic acid	56.09	3513.09	1.18 ± 0.03
22	3α,5α-Cyclo-ergosta-7,9(11),22-triene-6β-ol isomer 2	56.27	3479.49	0.60 ± 0.02

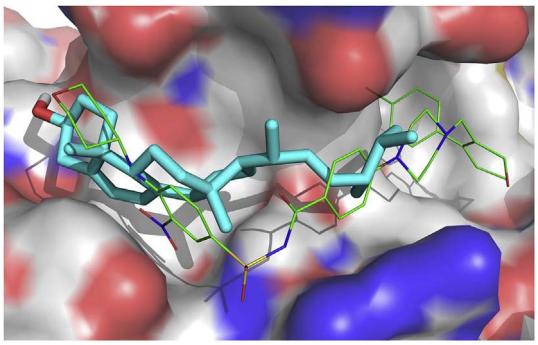

Fig. 8. Representation of Bcl-2 structure with docking conformation of Ergosta-5,7,22-trien-3β (cyan color, sticks and balls representation) and the co-crystallized inhibitor Venetoclax (green color, wire representation). Representation prepared using Pymol. (For interpretation of the references to color in this figure legend, the reader is referred to the Web version of this article.)

detected in the negative control (Fig. 2), while early-stages of apoptosis, marked by crescent-shaped or granular yellow green AO nuclear staining, were detected after cell exposition to 0.025 mg/mL of the extract (Fig. 2B). Late-stage of apoptosis, with condensation of chromatin, was observed after 0.05 mg/mL exposition, as indicated by localized orange and red nuclear EB staining (Fig. 2 C). All necrotic cells increased in volume and showed red fluorescence at their periphery.

To further analyze the effect of the PSC-hex in promoting apoptosis, the Annexin V and PI staining assay was performed (Fig. 3). After exposition to PSC-hex, the number of HCT116^{wt} cells in early apoptosis increased from 0,45% (Fig. 3A, **control**), to 65,6% (Fig. 3C, **0.05 mg/mL);** while the number of viable cells decreased from 92,2% (Fig. 3A, **control**), to 25,9% (Fig. 3C, **0.05 mg/mL)**. Both staining protocols confirm that PSC-hex exerts the observed cytotoxicity, at least partially, through a pro-apoptotic pathway.

Analysis of the effect of PSC-hex on HCT116^{wt} cell cycle was also performed by flow cytometry and results show an increase of cells in the G2/M transition phase, with a concomitant decrease of cells in the G1 and S-phases (Fig. 4). PSC-hex therefore seems to be an inducer of G2/M cell cycle arrest. A significant accumulation of cells in the sub-G1 fraction was also observed, indicating that the extract induces apoptosis (Fig. 4D).

3.3. PSC-hex activated depolarization of the mitochondrial membrane potential and ROS accumulation in HCT116^{wt} cells

The loss of Mitochondrial Membrane Potential (ΔΨm) is usually an indicator of changes in the permeability of the mitochondrial membrane, a process that is regulated by the Bcl-2 protein family (Ashkenazi et al., 2017). In addition to the loss of ΔΨm, changes in permeability can lead to the release of apoptosis factors such as cytochrome c, which triggers the activation of caspase-9 followed by activation of effector caspase-3, finally leading to apoptosis (Birkinshaw and Czabotar, 2017). The study of possible fluctuations in △Ψm in the presence of PSC-hex was thus performed by flow cytometry, using the DiOC6(3) stain protocol (Fig. 5). Compared with the untreated control (Fig. 5A), both 0.025 and 0.05 mg/mL PSC-hex concentrations (Fig. 5B–C) promoted a decrease in fluorescence, indicating an induced ΔΨm depolarization in HCT116^{wt} cells. These results suggest that PSC-hex might be promoting apoptosis through pathways associated with increase in mitochondrial permeability.

Cellular ROS production has been suggested as a possible cause for ΔΨm depolarization and subsequent induction of apoptosis and cell death (Chang et al., 2017). Many chemotherapeutic agents may be selectively toxic to tumor cells, because they increase oxidant stress beyond tumor cell support (Lee et al., 2016). Previous studies indicate that production of ROS is a relevant factor for regulating apoptosis (Al-Khayal et al., 2017; Hu et al., 2016). To investigate if the mitochondrial dysfunction observed in HCT116^{wt} cells is promoted by ROS production, a flow cytometry assay using DCF-DA stain was used to measure ROS levels. As shown in Fig. 6, the levels of H_2O_2 and $O_2^{\bullet -}$ in cells treated with 0.025 mg/mL and 0.05 mg/mL of PSC-hex, were elevated by 3-fold and 2-fold respectively, compared to the untreated control cells. These results indicate that apoptosis induced by PSC-hex may be strongly associated with ROS accumulation.

3.4. Intrinsic signaling pathway modulated apoptosis in HCT116^{wt} cells

To investigate the pathways by which PSC-hex may inducing apoptosis in HCT116^{wt}, we performed determination of apoptosis-related proteins using the Proteome Profiler Array (Human Apoptosis Antibody Array Kit, Abcam, #ab13400). HCT116^{wt} cells exposed to 0.05 mg/mL of PSC-hex, showed a significantly altered expression profile of apoptosis-related proteins. Increased expression was observed for several apoptotic related proteins including Fas, HSP 60, HSP 70, Xiap, HTRA, Survivin, Smac, caspase-3, Cytochrome-c, p53, Bax, Bad, Bid and Bim (Fig. 7A and B).

To confirm and validate the protein array results, the expression levels of Bax, Bcl-2, caspase-3 and p53 was further determined using western blot analysis. The results indicate up-regulation of Caspase-3, Bax and p53, while Bcl-2 showed down-regulation in HCT116^{wt} (Fig. 7C). p53 has been shown to play a critical role in intrinsic tumor suppression pathways, via apoptosis induction and cell cycle arrest pathways (Napoli and Flores, 2017). One of the multiple effects of p53 is to promote apoptosis by disrupting the Bax/Bcl-2 complex and consequent activation of caspase 3. The observed increase in Bax and p53 expression and decrease Bcl-2 expression, provides evidence that the PSC-hex probably promotes its pro-apoptotic activity by activating the p53 mediated pro-apoptotic pathway. This assumption is corroborated by the observed decrease in ΔΨm, a wallmark in p53 mediated induction of apoptosis. For cell cycle arrest, p53 exerts its effects through

cyclin-dependent kinase (CDK) inhibitor p21, leading to cell cycle arrest (Kim et al., 2017). Cell cycle analysis showed that PSC-hex induced cell cycle arrest at the G2/M phase, suggesting a blockage of cell proliferation of the HCT116^{wt}, which might be regulated by p53 by activating p21. This assumption is corroborated by the absence of cytotoxicity when HTC116^{-p21}, HTC116^{-p53} and HTC116^{-Bax} cells were used.

3.5. Chemical composition of PSC-hex

Table 1 shows the results regarding the identification and relative percentage of the twenty-two volatile compounds present in the PSC-hex. All compounds were identified with tetradecanoic acid (myristic acid, C14:0), pentadecanoic acid (C15:0), hexadecanoic acid (palmitic acid, C16:0), 9,12-octadecadienoic acid (linoleic acid, C18:2) and ergosta-5,7,22-trien-3β-ol being the main compounds identified in the extract, with the latter one as most abundant (30.6% of total compounds). These results are in accordance with those previously reported by others authors studying a similar extract from the *Pleurotus ostreatus* (Priya et al., 2012; Mohamed and Farghaly, 2014). Kayode et al. (2015) identified fatty acids and Usami et al. (2014) other types of compounds, mainly volatile, in *Pleurotus sajor-caju*.

3.6. Docking simulation of ergosta-5,7,22-trien-3β against Bcl-2

Bcl-2 is a well-known therapeutic target for anti-tumoral compounds. Known inhibitors promote apoptosis by occupying a hydrophobic cleft in the Bcl-2 structural thus preventing binding of Bcl-2 to pro-apoptotic protein partners including Bax (Radha and Raghavan, 2017). PSC-hex has shown to induce apoptosis by regulating expression of several apoptotic-related proteins, including down-regulating on of Bcl-2 expression. However an alternative pathway for inducing apoptosis might be accomplished by direct interaction of the compounds observed in PSC-hex with Bcl-2 (Table 1). Because ergosta-5,7,22-trien-3β comprises 30% of the extract content, we performed *in silico* docking simulations of this compound against Bcl-2, targeting the hydrophobic interaction cleft. The ergosta-5,7,22-trien-3β docked conformation fitted nicely in the Bcl-2 hydrophobic cleft, in a similar fashion to Venetoclax, a known Bcl-2 inhibitor (Fig. 8) (Souers et al., 2013), with an experimental IC_{50} value of 58 nM and currently in clinical trials against different types of tumors (Cang et al., 2015). Ergosta-5,7,22-trien-3β only interacts with a partial section of the hydrophobic cleft, so we do not expect its inhibition ability to be as high as Venetoclax, still this docking analysis demonstrate that activation of apoptosis by PSC-hex may be, at least partially, through direct inhibition of Bcl-2 by ergosta-5,7,22-trien-3β.

4. Conclusion

PSC-hex was able to generate several molecular responses on HCT116^{wt} colorectal cancer cell line, such as inducing initial apoptosis through the intrinsic pathway with upregulation of caspase-3 and Bax, with cell cycle arrest in G2/M, ROS accumulation and mitochondrial membrane depolarization. *P. sajor-caju* can emerge as an important nutraceutical and pharmacological natural source, in which steroid compounds appear to play a role on the observed cytotoxic and apoptotic effects here reported.

Due to the clinical and molecular heterogeneity of CRC, therapeutic modalities with new approaches to cancer therapy are essential. Many tumors have defects in activation of apoptosis because of overexpression of Bcl-2 pro-survival proteins or by inactivation of the p53 pathway (Adams and Cory, 2018). There is evidence that mushroom extracts have direct cytotoxic effects on cancer cells, which partially explains the *in vivo* effect on reducing tumor growth and anti-metastasis effect (Arata et al., 2016; Tangen et al., 2015). One of the mechanisms is induction of apoptosis through the mitochondrial pathway, increasing Bax and decreasing Bcl-2 expression (Liang et al., 2014). Because extracts act on this signaling pathway, nanotechnology can be used to pack mushroom extracts for more efficient delivery. Another alternative is dietary supplements in combination with conventional therapy. The use of combined therapy works on multiple metabolic pathways: it reduces the development of resistance to anticancer drugs, increases the sensitivity to the effect of chemotherapeutics, reinforcing the effectiveness of concentrations and minimizes adverse effects.

Conflicts of interest

The authors declare no conflicts of interest.

Acknowledgments

The authors thank Dr. Larsen (Institut National de la Santé et de la Recherche Médicale) for the gift of HCT116^{-Bax}, HCT116^{-p21} and HCT116^{-p53} cells. The authors are grateful to the Foundation for Science and Technology (FCT, Portugal) and FEDER under Programme PT2020 for financial support to CIMO (UID/AGR/00690/2013) and L. Barros contract. T.C. Finimundy thanks CAPES Foundation, Ministry of Education of Brazil (CAPES fellow, process number 88881.134581/2016–01). This work is supported by a grant from Coordenação de Aperfeiçoamento de Pessoal de Nível Superior (CAPES) and Fundação de Amparo à Pesquisa do Estado do Rio Grande do Sul (FAPERGS).

Transparency document

Transparency document related to this article can be found online at http://dx.doi.org/10.1016/j.fct.2018.01.015.

References

Adams, J.M., Cory, S., 2018. The BCL-2 arbiters of apoptosis and their growing role as cancer targets. Cell Death Differ. 25, 27–36.
Al-Khayal, K., Alafeefy, A., Vaali-Mohammed, M.A., Mahmood, A., Zubaidi, A., Al-Obeed, O., Khan, Z., Abdulla, M., Ahmad, R., 2017. Novel derivative of aminobenzenesulfonamide (3c) induces apoptosis in colorectal cancer cells through ROS generation and inhibits cell migration. BMC Canc. 17, 4.
Alonso, E.N., Ferronato, M.J., Gandini, N.A., Fermento, M.E., Obiol, D.J., Lopez Romero, A., Arevalo, J., Villegas, M.E., Facchinetti, M.M., Curino, A.C., 2017. Antitumoral effects of d-fraction from grifola frondosa (maitake) mushroom in breast cancer. Nutr. Canc. 69, 29–43.
Aranda, A., Sequedo, L., Tolosa, L., Quintas, G., Burello, E., Castell, J.V., Gombau, L., 2013. Dichloro-dihydro-fluorescein diacetate (DCFH-DA) assay: a quantitative method for oxidative stress assessment of nanoparticle-treated cells. Toxicol. Vitro: Int. J. Publ. Assoc. BIBRA 27, 954–963.
Arata, S., Watanabe, J., Maeda, M., Yamamoto, M., Matsuhashi, H., Mochizuki, M., Kagami, N., Honda, K., Inagaki, M., 2016. Continuous intake of the Chaga mushroom (Inonotus obliquus) aqueous extract suppresses cancer progression and maintains body temperature in mice. Heliyon 2, e00111.
Arnold, M., Sierra, M.S., Laversanne, M., Soerjomataram, I., Jemal, A., Bray, F., 2017. Global patterns and trends in colorectal cancer incidence and mortality. Gut 66, 683–691.
Ashkenazi, A., Fairbrother, W.J., Leverson, J.D., Souers, A.J., 2017. From basic apoptosis discoveries to advanced selective BCL-2 family inhibitors. Nat. Rev. Drug Discov. 16, 273–284.
Assis, I.S., Chaves, M.B., Silveira, M.L.L., Gern, R.M.M., Wisbeck, E., Furigo, A., Furlan, S.A., 2013. Production of bioactive compounds with antitumor activity against sarcoma 180 by Pleurotus sajor-caju. J. Med. Food 16, 1004–1012.
Bahrami, A., Khazaei, M., Hassanian, S.M., 2018. Targeting the tumor microenvironment as a potential therapeutic approach in colorectal cancer. Ration. Prog. 233, 2928–2936.
Barreira, J.C.M., Ferreira, I.C.F.R., 2015. Steroids in Natural Matrices, Biotechnology of Bioactive Compounds. John Wiley & Sons, Ltd, pp. 395–431.
Berg, K.C.G., Eide, P.W., Eilertsen, I.A., Johannessen, B., Bruun, J., Danielsen, S.A., Bjornslett, M., Meza-Zepeda, L.A., Eknaes, M., Lind, G.E., Myklebost, O., Skotheim, R.I., Sveen, A., Lothe, R.A., 2017. Multi-omics of 34 colorectal cancer cell lines - a resource for biomedical studies. Mol. Canc. 16, 116.
Birkinshaw, R.W., Czabotar, P.E., 2017. The BCL-2 family of proteins and mitochondrial outer membrane permeabilisation. Semin. Cell Dev. Biol. 72, 152–162. http://dx.doi.org/10.1016/j.semcdb.2017.04.001.
Cang, S., Iragavarapu, C., Savooji, J., Song, Y., Liu, D., 2015. ABT-199 (venetoclax) and BCL-2 inhibitors in clinical development. J. Hematol. Oncol. 8, 129.
Carpentier, G.H.E., 2014. Protein array analyzer for ImageJ. In: Carpentier, G. (Ed.), Centre de Recherche Public Henri Tudor, pp. 5.
Chang, C.T., Korivi, M., Huang, H.C., Thiyagarajan, V., Lin, K.Y., Huang, P.J., Liu, J.Y.,

Hseu, Y.C., Yang, H.L., 2017. Inhibition of ROS production, autophagy or apoptosis signaling reversed the anticancer properties of Antrodia salmonea in triple-negative breast cancer (MDA-MB-231) cells. Food Chem. Toxicol.: Int. J. Publ. Br. Ind. Biol. Res. Assoc. 103, 1–17.
Delano, W.L., 2002. The PyMOL Molecular Graphics System.
Denizot, F., Lang, R., 1986. Rapid colorimetric assay for cell growth and survival. Modifications to the tetrazolium dye procedure giving improved sensitivity and reliability. J. Immunol. Meth. 89, 271–277.
Falcão, S.I., Freire, C., Figueiredo, A.C., Boas, M.V., 2016. The volatile composition of Portuguese propolis towards its origin discrimination. Record Nat. Prod. 10.
Ferreira, I.C., Vaz, J.A., Vasconcelos, M.H., Martins, A., 2010. Compounds from wild mushrooms with antitumor potential. Anti Canc. Agents Med. Chem. 10, 424–436.
Gogavekar, S.S., Rokade, S.A., Ranveer, R.C., Ghosh, J.S., Kalyani, D.C., Sahoo, A.K., 2014. Important nutritional constituents, flavour components, antioxidant and antibacterial properties of Pleurotus sajor-caju. J. Food Sci. Technol. 51, 1483–1491.
Greeshma, P., Ravikumar, K.S., Neethu, M.N., Pandey, M., Zuhara, K.F., Janardhanan, K.K., 2016. Antioxidant, anti-inflammatory, and antitumor activities of cultured mycelia and fruiting bodies of the elm oyster mushroom, hypsizygus ulmarius (agaricomycetes). Int. J. Med. Mushrooms 18, 235–244.
Heleno, S.A., Diz, P., Prieto, M.A., Barros, L., Rodrigues, A., Barreiro, M.F., Ferreira, I.C.F.R., 2016. Optimization of ultrasound-assisted extraction to obtain mycosterols from Agaricus bisporus L. by response surface methodology and comparison with conventional Soxhlet extraction. Food Chem. 197, 1054–1063.
Heleno, S.A., Martins, A., Queiroz, M.J., Ferreira, I.C., 2015. Bioactivity of phenolic acids: metabolites versus parent compounds: a review. Food Chem. 173, 501–513.
Hird, A.W., Aquila, B.M., Hennessy, E.J., Vasbinder, M.M., Yang, B., 2015. Small molecule inhibitor of apoptosis proteins antagonists: a patent review. Expert Opin. Ther. Pat. 25, 755–774.
Hu, L., Wang, H., Huang, L., Zhao, Y., Wang, J., 2016. The protective roles of ROS-mediated mitophagy on 125I seeds radiation induced cell death in HCT116 cells. Oxidative Med. Cell. Longev. 2016, 9460462.
Jin, X., Ruiz Beguerie, J., Sze, D.M., Chan, G.C., 2016. Ganoderma lucidum (Reishi mushroom) for cancer treatment. Cochrane Database Syst. Rev. 4, CD007731.
Joana Gil-Chávez, G., Villa, J.A., Fernando Ayala-Zavala, J., Basilio Heredia, J., Sepulveda, D., Yahia, E.M., González-Aguilar, G.A., 2013. Technologies for extraction and production of bioactive compounds to be used as nutraceuticals and food ingredients: an overview. Compr. Rev. Food Sci. Food Saf. 12, 5–23.
Kalyanaraman, B., Cheng, G., Hardy, M., Ouari, O., Lopez, M., Joseph, J., Zielonka, J., Dwinell, M.B., 2018. A review of the basics of mitochondrial bioenergetics, metabolism, and related signaling pathways in cancer cells: therapeutic targeting of tumor mitochondria with lipophilic cationic compounds. Redox Biol. 14, 316–327.
Kayode, R.M.O., Olakulehin, T.F., Adedeji, B.S., Ahmed, O., Aliyu, T.H., Badmos, A.H.A., 2015. Evaluation of amino acid and fatty acid profiles of commercially cultivated oyster mushroom (Pleurotus sajor-caju) grown on gmelina wood waste. Niger. Food J. 33, 18–21.
Kikuchi, T., Motoyashiki, N., Yamada, T., Shibatani, K., Ninomiya, K., Morikawa, T., Tanaka, R., 2017. Ergostane-type sterols from king trumpet mushroom (Pleurotus eryngii) and their inhibitory effects on aromatase. Int. J. Mol. Sci. 18.
Kim, E.M., Jung, C.H., Kim, J., Hwang, S.G., Park, J.K., Um, H.D., 2017. The p53/p21 complex regulates cancer cell invasion and apoptosis by targeting Bcl-2 family proteins. Canc. Res. 77, 3092–3100. http://dx.doi.org/10.1158/0008-5472.CAN-16-2098.
Lee, M.H., Hong, S.H., Park, C., Kim, G.Y., Leem, S.H., Choi, S.H., Keum, Y.S., Hyun, J.W., Kwon, T.K., Hong, S.H., Choi, Y.H., 2016. Hwang-Heuk-San induces apoptosis in HCT116 human colorectal cancer cells through the ROS-mediated activation of caspases and the inactivation of the PI3K/Akt signaling pathway. Oncol. Rep. 36, 205–214.
Liang, Z., Guo, Y.T., Yi, Y.J., Wang, R.C., Hu, Q.L., Xiong, X.Y., 2014. Ganoderma lucidum polysaccharides target a Fas/caspase dependent pathway to induce apoptosis in human colon cancer cells. Asian Pac. J. Cancer Prev. APJCP 15, 3981–3986.
Liu, K., Liu, P.C., Liu, R., Wu, X., 2015. Dual AO/EB staining to detect apoptosis in osteosarcoma cells compared with flow cytometry. Med. Sci. Monit. Basic Res. 21, 15–20.
Lo, H.C., Hsu, T.H., Lin, F.Y., Wasser, S.P., Chen, Y.H., Lee, C.H., 2012. Effects of yellow brain culinary-medicinal mushroom, Tremella mesenterica Ritz.:Fr. (higher Basidiomycetes), on immune function in normal and type 1 diabetic rats. Int. J. Med. Mushrooms 14, 447–457.
Mohamed, E.M., Farghaly, F.A., 2014. Bioactive compounds of fresh and dried *Pleurotus Ostreatus* mushroom. Int. J. Biotechnol. Wellness Ind. 3, 4–14. http://dx.doi.org/10.6000/1927-3037.2014.03.01.2.
Monks, A., Scudiero, D., Skehan, P., Shoemaker, R., Paull, K., Vistica, D., Hose, C., Langley, J., Cronise, P., Vaigro-Wolff, A., et al., 1991. Feasibility of a high-flux anticancer drug screen using a diverse panel of cultured human tumor cell lines. J. Nat. Canc. Inst. 83, 757–766.
Morris, G.M., Huey, R., Olson, A.J., 2008. Using AutoDock for ligand-receptor docking. Curr. Prot. Bioinf. Chapter 8, 1–40. http://dx.doi.org/10.1002/0471250953.bi0814s24.
Napoli, M., Flores, E.R., 2017. The p53 family orchestrates the regulation of metabolism: physiological regulation and implications for cancer therapy. Br. J. Canc. 116, 149–155.
Opferman, J.T., Kothari, A., 2018. Anti-apoptotic BCL-2 family members in development. Cell Death Differ. 25, 37–45.
Pajaniradje, S., Mohankumar, K., Pamidimukkala, R., Subramanian, S., Rajagopalan, R., 2014. Antiproliferative and apoptotic effects of Sesbania grandiflora leaves in human cancer cells. BioMed Res. Int. 2014, 474953.
Pedretti, A., Villa, L., Vistoli, G., 2004. VEGA - an open platform to develop chemo-bioinformatics applications, using plug-in architecture and script programming. J. Comput. Aided Mol. Des. 18, 6.
Pietkiewicz, S., Schmidt, J.H., Lavrik, I.N., 2015. Quantification of apoptosis and necroptosis at the single cell level by a combination of Imaging Flow Cytometry with classical Annexin V/propidium iodide staining. J. Immunol. Meth. 423, 99–103.
Pozarowski, P., Darzynkiewicz, Z., 2004. Analysis of cell cycle by flow cytometry. Meth. Mol. Biol. 281, 301–311.
Priya, V., Jananie, R.K., Vijayalakshmi, K., 2012. GC/MS determination of bioactive components of *Pleurotus ostreatus*. Int. Res. J. Pharm. 3, 150–151. http://dx.doi.org/10.7897/2230-8407.
Quidde, J., Hegewisch-Becker, S., Graeven, U., Lerchenmuller, C.A., Killing, B., Depenbusch, R., Steffens, C.C., Lange, T., Dietrich, G., Stoehlmacher, J., Reinacher, A., Tannapfel, A., Trarbach, T., Marschner, N., Schmoll, H.J., Hinke, A., Al-Batran, S.E., Arnold, D., 2016. Quality of life assessment in patients with metastatic colorectal cancer receiving maintenance therapy after first-line induction treatment: a preplanned analysis of the phase III AIO KRK 0207 trial. Ann. Oncol.: Off. J. Eur. Soc.Med. Oncol. 27, 2203–2210.
Radha, G., Raghavan, S.C., 2017. BCL2: a promising cancer therapeutic target. Biochim. Biophys. Acta Rev. Canc 1868, 309–314.
Rejhová, A., Opattová, A., Čumová, A., Slív, D., Vodička, P., 2017. Natural compounds and combination therapy in colorectal cancer treatment. Eur. J. Med. Chem. 144, 582–594. http://dx.doi.org/10.1016/j.ejmech.2017.12.039.
Ren, L., Perera, C., Hemar, Y., 2012. Antitumor activity of mushroom polysaccharides: a review. Food Funct. 3, 1118–1130.
Rodriguez-Salas, N., Dominguez, G., Barderas, R., Mendiola, M., García-Albéniz, X., Maurel, J., Batlle, J.F., 2017. Clinical relevance of colorectal cancer molecular subtypes. Crit. Rev. Oncol.-Hematol. 109, 9–19.
Roncero-Ramos, I., Delgado-Andrade, C., 2017. The beneficial role of edible mushrooms in human health. Curr. Opin. Food Sci. 14, 122–128.
Sang, S., Ju, J., Lambert, J.D., Lin, Y., Hong, J., Bose, M., Wang, S., Bai, N., He, K., Reddy, B.S., Ho, C.T., Li, F., Yang, C.S., 2006. Wheat bran oil and its fractions inhibit human colon cancer cell growth and intestinal tumorigenesis in Apc(min/+) mice. J. Agric. Food Chem. 54, 9792–9797.
Santesso, N., Wieland, L.S., 2016. A summary of a cochrane review: ganoderma lucidum (reishi mushroom) for the treatment of cancer. Eur. J. Integr. Med. 8, 619–620.
Schneider, C.A., Rasband, W.S., Eliceiri, K.W., 2012. NIH Image to ImageJ: 25 years of image analysis. Br. J. Pharmacol. 9, 671–675.
Souers, A.J., Leverson, J.D., Boghaert, E.R., Ackler, S.L., Catron, N.D., Chen, J., Dayton, B.D., Ding, H., Enschede, S.H., Fairbrother, W.J., Huang, D.C., Hymowitz, S.G., Jin, S., Khaw, S.L., Kovar, P.J., Lam, L.T., Lee, J., Maecker, H.L., Marsh, K.C., Mason, K.D., Mitten, M.J., Nimmer, P.M., Oleksijew, A., Park, C.H., Park, C.M., Phillips, D.C., Roberts, A.W., Sampath, D., Seymour, J.F., Smith, M.L., Sullivan, G.M., Tahir, S.K., Tse, C., Wendt, M.D., Xiao, Y., Xue, J.C., Zhang, H., Humerickhouse, R.A., Rosenberg, S.H., Elmore, S.W., 2013. ABT-199, a potent and selective BCL-2 inhibitor, achieves antitumor activity while sparing platelets. Nat. Med. 19, 202–208.
Tanaka, A., Nishimura, M., Sato, Y., Sato, H., Nishihira, J., 2016. Enhancement of the Th1-phenotype immune system by the intake of Oyster mushroom (Tamogitake) extract in a double-blind, placebo-controlled study. J. Tradit. Chin. Med. 6, 424–430.
Tangen, J.-M., Tierens, A., Caers, J., Binsfeld, M., Olstad, O.K., Trøseid, A.-M.S., Wang, J., Tjønnfjord, G.E., Hetland, G., 2015. Immunomodulatory effects of the agaricus blazei murrill-based mushroom extract AndoSan in patients with multiple myeloma undergoing high dose chemotherapy and autologous stem cell transplantation: a randomized, double blinded clinical study. BioMed Res. Int. 2015, 718539.
Tolosa, L., Donato, M.T., Gomez-Lechon, M.J., 2015. General cytotoxicity assessment by means of the MTT assay. Meth. Mol. Biol. 1250, 333–348.
Trott, O., Olson, A.J., 2010. AutoDock Vina: improving the speed and accuracy of docking with a new scoring function, efficient optimization, and multithreading. J. Comput. Chem. 31, 455–461.
Usami, A., Nakaya, S., Nakahashi, H., Miyazawa, M., 2014. Chemical composition and aroma evaluation of volatile oils from edible mushrooms (Pleurotus salmoneostramineus and Pleurotus sajor-caju). J. Oleo Sci. 63, 1323–1332.
Venkatesh Gobi, V., Rajasankar, S., Ramkumar, M., Dhanalakshmi, C., Manivasagam, T., Justin Thenmozhi, A., Essa, M.M., Chidambaram, R., 2018. Agaricus blazei extract attenuates rotenone-induced apoptosis through its mitochondrial protective and antioxidant properties in SH-SY5Y neuroblastoma cells. Nutr. Neurosci. 21, 97–107.
Villares, A., García-Lafuente, A., Guillamón, E., Ramos, Á., 2012. Identification and quantification of ergosterol and phenolic compounds occurring in Tuber spp. truffles. J. Food Compos. Anal. 26, 177–182.
Wlodkowic, D., Skommer, J., Darzynkiewicz, Z., 2009. Flow cytometry-based apoptosis detection. Methods Mol. Biol. 559, 19–32. http://dx.doi.org/10.1007/978-1-60327-017-5_2.
Yang, M., Wang, H., Zhou, M., Liu, W., Kuang, P., Liang, H., Yuan, Q., 2016. The natural compound sulforaphene, as a novel anticancer reagent, targeting PI3K-AKT signaling pathway in lung cancer. Oncotarget 7, 76656–76666.